Effect of Pressure on the Metal-Insulator Transition of the Cubic Pyrochlore $Tl_2Ru_2O_7$

Yuanyuan Jiao[1,2], Ziyi Liu[2,3], Ningning Wang[2,3], Bosen Wang[2,3], Jianping Sun[2,3*], and Jinguang Cheng[2,3*]

[1]*Faculty of Science, Wuhan University of Science and Technology, Wuhan 430062, China*
[2]*Beijing National Laboratory for Condensed Matter Physics, Institute of Physics, Chinese Academy of Sciences, Beijing 100190, China*
[3]*School of Physical Sciences, University of Chinese Academy of Sciences, Beijing 100190, China*

(Received 11 March 2025; accepted manuscript online 17 April 2025)

The cubic pyrochlore $Tl_2Ru_2O_7$ undergoes concurrently a metal–insulator transition (MIT) and a first-order structural transition at $T_{\rm MIT} \approx 120$ K, below which the system was found to form one-dimensional spin-one Haldane chains associated with an orbital ordering of Ru-4d electrons. With an aim to tune and access distinct ground states with strong entanglements of multiple degrees of freedom, i.e., spin, orbital, charge, and lattice, we utilize a high-pressure approach to regulate the MIT of this system. Our detailed resistivity $\rho(T)$ measurements on the polycrystalline $Tl_2Ru_2O_7$ samples under various hydrostatic pressures indeed reveal an unusual evolution of the electronic ground states. At first, the MIT is suppressed monotonically from 120 K at ambient to about 70 K at 1.5 GPa and then vanishes suddenly at about 1.8 GPa without achieving a metallic ground state. Meanwhile, the system evolves into a semiconducting ground state with magnitude of $\rho(T)$ in the entire temperature range enhanced gradually by further increasing pressure. Prior to the abrupt disappearance of MIT, a new electronic order manifested as a kink-like anomaly in $\rho(T)$ emerges at $T_0 > T_{\rm MIT}$ at 1.2 GPa and it continues to increase with pressure, producing a tricritical-point-like behavior in the T–P phase diagram of $Tl_2Ru_2O_7$. The presence of two successive transitions at T_0 and $T_{\rm MIT}$ in the pressure range 1.2–1.5 GPa indicates an inhomogeneous electronic state nearby the tricritical point. At $P \geq 3$ GPa, another broad anomaly emerges in $\rho(T)$ at $T_1 > T_0$, and T_1 continuously increases with pressure, dividing the semiconducting $\rho(T)$ into distinct thermally activated regions. These rich phenomena in the pressurized $Tl_2Ru_2O_7$ should originate from the complex interplay of strongly entangled multiple quantum degrees of freedom in the system near the localized-to-itinerant crossover regime.

DOI: 10.1088/0256-307X/42/5/057404 CSTR: 32039.14.0256-307X.42.5.057404

1. Introduction. The crossover between localization and itinerancy of strongly correlated electrons in transition-metal oxides (TMOs) leads to many exotic phenomena such as unconventional superconductivity, quantum criticality, and metal–insulator transition. These phenomena are characterized by strong entanglement of charge, spin, orbital, and lattice degrees of freedom.[1–11] Compared to the 3d TMOs, the 4d counterparts are featured by spatially more extended 4d orbitals and enhanced spin-orbital coupling λ. In addition, the comparable energy scales of Coulomb repulsion U and bandwidth W place the 4d TMOs closer to the localized-to-itinerant electron crossover regime, making them easier for electronic state regulations by applying external stimuli such as high pressure P.[12–15]

Among the 4d TMOs, $Tl_2Ru_2O_7$ with the pyrochlore structure stands out as a unique system that exhibits rich phenomena and distinct physical properties in comparison with other Ru^{4+} pyrochlore ruthenates.[15–24] For example, $Tl_2Ru_2O_7$ displays a sharp metal–insulator transition (MIT) in resistivity $\rho(T)$ at $T_{\rm MIT} \approx 120$ K,[4,24] while the rare-earth ruthenates $R_2Ru_2O_7$ (R = Pr-Lu, Y) are insulators[20,21] and the $Bi_2Ru_2O_7$ exhibits a metallic behavior.[22,23] In addition, the Tl-NMR study on $Tl_2Ru_2O_7$ reveals a nonmagnetic spin-singlet ground state with a spin gap between the ground state and excited states,[24] while a long-range magnetic order of the Ru^{4+} spins was confirmed by powder neutron diffraction in the $R_2Ru_2O_7$.[19] Further investigations on $Tl_2Ru_2O_7$ have revealed a strong coupling of multiple quantum degrees of freedom in this system. It was found that the MIT at $T_{\rm MIT}$ is accompanied by a concurrent first-order cubic-orthorhombic structural transition, which involves significant changes of local structures, in particular the Ru-O bond lengths that split into two distinct groups below $T_{\rm MIT}$.[4] Such a structural modification has been attributed to the orbital ordering of Ru 4d electrons, which was further proposed to produce one-dimensional spin-one Haldane chains with spin gap below $T_{\rm MIT}$.[4] In addition, optical conductivity and photoemission spectroscopy studies evidenced the self-doping effect on the electronic states near the Fermi level from the Tl 6s states, which un-

*Corresponding author. Email: jpsun@iphy.ac.cn; jgcheng@iphy.ac.cn
© 2025 Chinese Physical Society and IOP Publishing Ltd. All rights, including for text and data mining, AI training, and similar technologies, are reserved.

dergoes significant renormalization below $T_{\rm MIT}$.[25] These characterizations thus demonstrated an intimated interplay among orbital, spin, charge, and lattice degrees of freedom in governing the MIT and spin-singlet insulating ground state of $Tl_2Ru_2O_7$.

Considering that this system is in close proximity to the localized-to-itinerant electron crossover, it should be interesting to explore how the highly correlated electronic states evolve when the MIT is suppressed by pressure. We noted that the application of high pressure can completely suppress the MIT of isostructural $Hg_2Ru_2O_7$ with $T_{\rm MIT} \approx 170\,{\rm K}$[20–22] at ambient pressure and realize a Fermi-liquid metallic state at approximately 5 GPa.[26,27] Whether a similar high-pressure approach is also effective in regulating the MIT of $Tl_2Ru_2O_7$ deserves exploration. To this end, we have synthesized the polycrystalline $Tl_2Ru_2O_7$ samples under 4 GPa and 1000 ℃ and confirmed its high quality by observing a sharp first-order MIT at $T_{\rm MIT} \approx 120\,{\rm K}$ in various physical properties. In comparison to $Hg_2Ru_2O_7$, our detailed high-pressure resistivity $\rho(T)$ measurements on $Tl_2Ru_2O_7$ revealed a distinct pressure effect of the MIT, which vanishes suddenly at about 1.8 GPa without achieving a metallic ground state. Interestingly, the system gradually evolves into a semiconducting ground state with characteristic anomalies in $\rho(T)$, signaling the emergence of new electronic orders that are further enhanced by pressure. Such an unusual evolution of the electronic ground states produces a tricritical-point-like behavior in the T–P phase diagram of $Tl_2Ru_2O_7$, which is an ideal platform to investigate the complex interplay of strongly entangled multiple quantum degrees of freedom near the localized-to-itinerant electron crossover.

2. Experimental Details. The $Tl_2Ru_2O_7$ polycrystalline samples used in the present study were synthesized under high-pressure and high-temperature (HPHT) conditions by using a Kawai-type multianvil module. A stoichiometric mixture of Tl_2O_3 and RuO_2 powders mixed with 30%wt. $KClO_4$ were sealed in a gold capsule and then subjected to HPHT reaction at 4 GPa and 1000 ℃ for 20 minutes. The samples recovered after releasing pressure were washed by deionized water to remove the remanent KCl. Then, we performed a second HPHT treated on the resultant $Tl_2Ru_2O_7$ powders by encapsuling them with $KClO_4$ on both ends in order to obtain a dense pellet for various physical properties measurements at ambient and high pressures.

The phase purity of the obtained $Tl_2Ru_2O_7$ polycrystalline samples was examined by powder X-ray diffraction (XRD) at room temperature. Temperature dependence of $\rho(T)$ at ambient pressure was measured with standard four-probe method by using the Physical Property Measurements System (PPMS, Quantum Design) in the temperature range of 2–300 K. DC magnetic susceptibility $\chi(T)$ was measured with a commercial Magnetic Property Measurements System (MPMS-III, Quantum Design) in the temperature rang of 2–300 K under an external magnetic field of $\mu_0 H = 0.1\,{\rm T}$.

The $\rho(T)$ under various pressures were measured with a piston cylinder cell (PCC) ($0 < P < 1.8\,{\rm GPa}$) and palm-type cubic anvil cell (CAC) ($2 \le P \le 8\,{\rm GPa}$).[4] The pressure values in PCC was determined from the superconducting transition temperature $T_{\rm c}$ of Pb according to the formula $P = [T_{\rm c}(0) - T_{\rm c}(P)]/0.365$ (P using the unit GPa) and the pressure in CAC was estimated from the calibration curve pre-determined by measuring the characteristic transitions of bismuth at room temperature. The high-pressure synchrotron XRD (SXRD) measurements were performed at the BL15U1 station in Shanghai Synchrotron Radiation Facility (SSRF) with a wavelength $\lambda = 0.6199\,$Å. The pressure was generated by using a diamond anvil cell (DAC) with 300 μm culet and the neon gas was used as pressure transmitting medium. We employ the ruby fluorescence method to calculate the pressure values in DAC. The SXRD data were analyzed with the FullProf program.

3. Results and Discussions. Rietveld refinements on the powder XRD patterns confirmed that the obtained $Tl_2Ru_2O_7$ samples are nearly single phase with the cubic $Fd\bar{3}m$ space group and lattice parameter $a \approx 10.18\,$Å, which is in general consistent with previous report.[13] Most samples were found to contain a trace amount of RuO_2 secondary phase, i.e., about 4–5%wt. Since RuO_2 is a paramagnetic metal, its presence will not affect the present study focusing on the sharp MIT. The high quality of obtained $Tl_2Ru_2O_7$ samples is further confirmed by pronounced anomalies around $T_{\rm MIT}$ in various physical properties shown in Fig. 1.

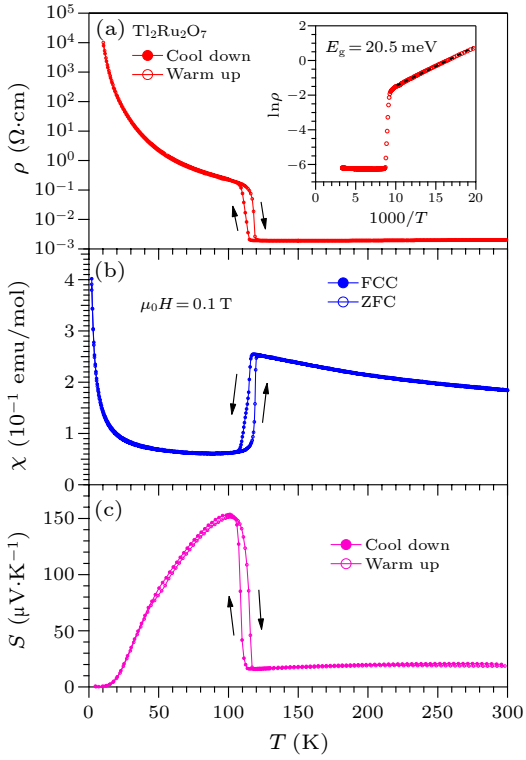

Fig. 1. Temperature dependences of (a) resistivity $\rho(T)$, (b) magnetic susceptibility $\chi(T)$, and (c) thermopower $S(T)$ of the $Tl_2Ru_2O_7$ polycrystalline samples. A pronounced first-order phase transition at $T_{\rm MIT} \approx 120\,{\rm K}$ can be clearly evidenced in the above physical properties.

Displayed in Fig. 1 are the temperature dependences of $\rho(T)$, $\chi(T)$, and thermopower $S(T)$ of $Tl_2Ru_2O_7$ upon thermal cycling in the temperature range of 2–300 K at ambient pressure. All these properties exhibit abrupt changes around $T_{MIT} \approx 120$ K with obvious thermal hysteresis, characteristic of a first-order phase transition. In specific, $\rho(T)$ shown in Fig. 1(a) exhibits a prominent MIT at $T_{MIT} \approx 120$ K, where the resistivity increases abruptly by two orders of magnitude from 10^{-3} to 10^{-1} Ω·cm upon cooling down. $\rho(T)$ above T_{MIT} shows a metallic behavior with weak temperature dependence, while $\rho(T)$ below T_{MIT} exhibits a typical semiconducting or insulating behavior with a dramatic increase by more than five orders of magnitude down to 10 K. As displayed in the inset of Fig. 1(a), $\rho(T)$ below T_{MIT} was analyzed with the thermal activation model, $\rho(T) = \rho_0 \exp(E_g/k_B T)$, yielding an energy gap of $E_g \approx 20.5$ meV at ambient pressure. On the other hand, $\chi(T)$ measured under $\mu_0 H = 0.1$ T also experiences an abrupt change at T_{MIT} from a Curie-Weiss-like behavior above T_{MIT} to a nearly temperature-independent behavior below T_{MIT} due to the formation of spin-singlet state,[26] while the low-temperature upturn tail should be attributed to the magnetic impurities or defects. A clear thermal hysteresis like $\rho(T)$ is also evidenced around T_{MIT} as shown in Fig. 1(b). Here, we estimate the effective magnetic moment of $Tl_2Ru_2O_7$ from the high-temperature susceptibility and the calculated $\mu_{eff} = 3.1\,\mu_B$/f.u. is close to the expected spin-only value of $S = 1$ for Ru^{4+}. In addition, the obtained $\theta_{CW} \sim -430$ K and $f \equiv |\theta_{CW}/T_{MIT}| \sim 3.6$ signal the presence of geometrical frustration in $Tl_2Ru_2O_7$ with pyrochlore structure.[4]

In addition to $\rho(T)$ and $\chi(T)$, we also measured thermopower $S(T)$ of $Tl_2Ru_2O_7$, which has not been reported so far to our knowledge. As seen in Fig. 1(c), $S(T)$ is positive in the whole temperature range and signals the dominant p-type charge carriers. With decreasing temperature, $S(T)$ first shows a weak temperature-dependent behavior and then suddenly exhibits a sharp jump at T_{MIT} from ∼20 μV/K to ∼160 μV/K. Such a dramatic change of $S(T)$ at MIT indicates a significant modification of the electronic density of states at Fermi level, consistent with the results from optical spectroscopy measurements.[28] Therefore, all these characterizations confirm high quality of the $Tl_2Ru_2O_7$ samples with a pronounced MIT at $T_{MIT} \approx 120$ K. Then, we can focus on the high-pressure resistivity measurements to investigate the evolutions of MIT and the corresponding electronic ground states as a function of pressure.

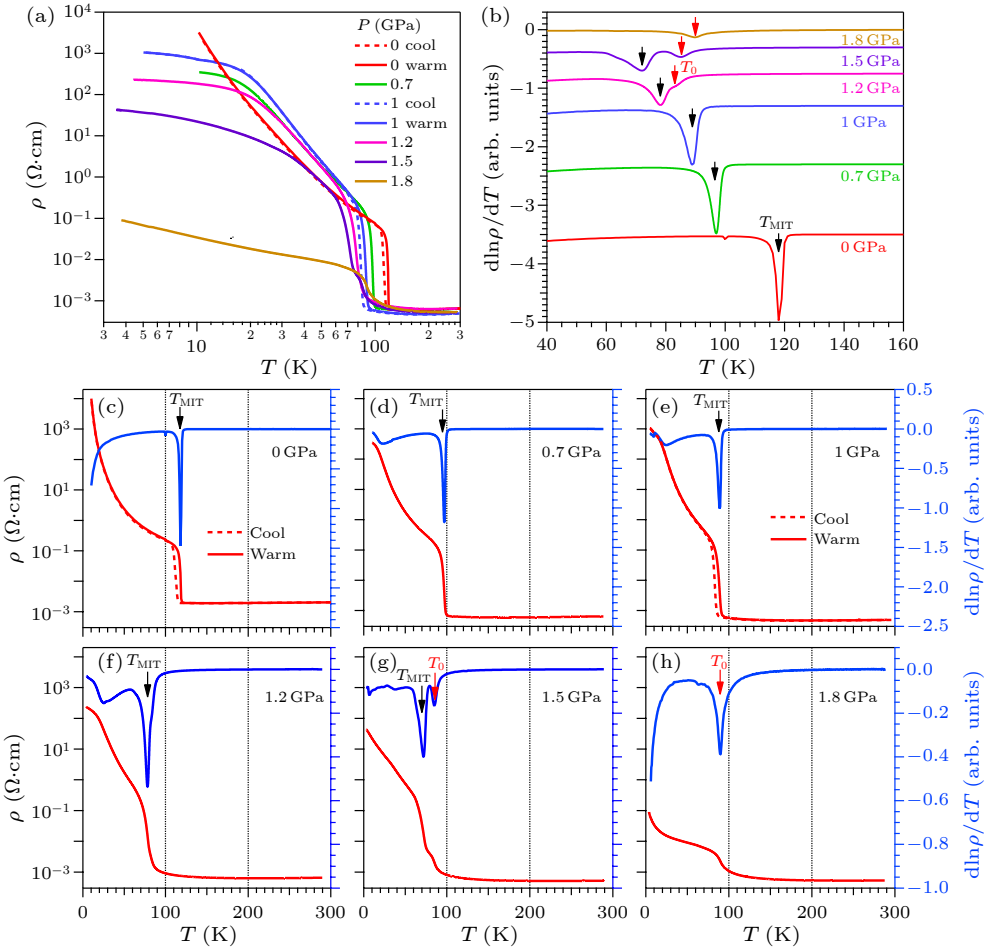

Fig. 2. Temperature dependences of (a) resistivity $\rho(T)$ and (b) the derivative $d\ln\rho/dT$ of $Tl_2Ru_2O_7$ under various hydrostatic pressures up to 1.8 GPa. For better tracking the corresponding phase transitions, temperature dependences of $\rho(T)$ and $d\ln\rho/dT$ at different pressures are shown in (c)–(h) for 0, 0.7, 1, 1.2, 1.5, and 1.8 GPa, respectively. The transitions at T_{MIT} and T_0 are marked by the down-pointing arrows with different colors.

We first measured $\rho(T)$ in a fine pressure interval up to 1.8 GPa by using PCC and shown all the results in Fig. 2(a). As can be seen, the MIT is gradually shifting to lower temperatures with increasing pressure, while the magnitude of $\rho(T)$ below $T_{\rm MIT}$ is first enhanced by pressure up to 1 GPa and then reduced quickly upon further increasing pressure. Unlike the continuous increase of $\rho(T)$ below $T_{\rm MIT}$ at 0 GPa, a resistivity plateau appears below ∼20 K at $P \geq 0.7$ GPa and its magnitude decreases dramatically by three orders of magnitude from 1.2 to 1.8 GPa. In addition to these general observations, a close inspection of $\rho(T)$ curves near the MIT revealed some interesting features and unusual evolutions of $T_{\rm MIT}$. To see these features and their evolutions clearly, we have replotted in Figs. 2(c)–2(h) the $\rho(T)$ curve in the logarithmic scale and its corresponding temperature derivative $\mathrm{d}\ln\rho/\mathrm{d}T$ at each pressure. A cascade plot of $\mathrm{d}\ln\rho/\mathrm{d}T$ curves at different pressures is given in Fig. 2(b).

As shown in Figs. 2(b) and 2(c), the abrupt jump of $\rho(T)$ at the MIT is manifested as a sharp dip in $\mathrm{d}\ln\rho/\mathrm{d}T$, from which we can determine $T_{\rm MIT} \approx 120$ K at 0 GPa. Upon increasing pressure gradually, $T_{\rm MIT}$ is suppressed monotonically to about 95, 87, 77, and 70 K for $P = 0.7, 1, 1.2$, and 1.5 GPa, respectively. Accordingly, the dip of $\mathrm{d}\ln\rho/\mathrm{d}T$ at $T_{\rm MIT}$ is also broadened up and diminished gradually. The thermal hysteresis remains visible at 1 GPa as shown in Fig. 2(e). Interestingly, prior to the MIT, $\rho(T)$ at 1.2 GPa exhibits a weak step-like anomaly at $T_0 \sim 83$ K, which is manifested as a kink or shallow dip in $\mathrm{d}\ln\rho/\mathrm{d}T$ [see Figs. 2(b) and 2(f)]. This feature is strengthened and the corresponding anomalies in $\rho(T)$ and $\mathrm{d}\ln\rho/\mathrm{d}T$ become clearer with a slight enhancement of T_0 to 85 K upon increasing pressure to 1.5 GPa [see Figs. 2(b) and 2(g)]. By tracking the evolutions of the magnitude of $\rho(T)$ and the anomalies in $\mathrm{d}\ln\rho/\mathrm{d}T$ up to 1.8 GPa, we surprisingly found that the MIT vanishes completely, and the electronic ground state below $T_0 \sim 85$ K remains a semiconducting behavior with reduced resistivity. These observations indicated the emergence of a new electronic order at T_0 above 1.2 GPa with a similar energy scale as the MIT in the pressurized $Tl_2Ru_2O_7$. The coexistence of T_0 and $T_{\rm MIT}$ in the pressure region 1.2–1.5 GPa signals an electronic inhomogeneity of this system.

To further track the evolution of T_0 at higher pressures, we performed resistivity measurements in CAC up to 8 GPa. As seen in Fig. 3(a), the $\rho(T)$ curve at 2 GPa in CAC is very similar to that at 1.8 GPa in PCC, confirming the reproducibility of above results. Below T_0, $\rho(T)$ shows a quick enhancement and this behavior is similar to $Cd_2Ru_2O_7$ under high pressures.[29] With increasing pressure to 8 GPa, $\rho(T)$ is enhanced monotonically in the whole temperature range, especially above T_0. According to the results of $\mathrm{d}\ln\rho/\mathrm{d}T$ in Fig. 3(b), the dip anomaly at T_0 shifts to higher temperatures gradually and its magnitude is significantly reduced with increasing pressure. Surprisingly, a second broad valley centered around $T_1 > T_0$ appears in $\mathrm{d}\ln\rho/\mathrm{d}T$, which reflects the slope change in $\rho(T)$. T_1 quickly moves to higher temperatures with pressure. Thus, $\rho(T)$ curves above 3 GPa were divided into two distinct thermal active regions above T_1 and below T_0. From the inset of Fig. 3(a), we can see that $\rho(T)$ below T_0 can be described by the three-dimensional variable range hopping (VRH) conduction, from which the activation energy gap is found to increase with pressure. These results revealed further modification of the electronic states in $Tl_2Ru_2O_7$ upon compression, demonstrating a complex evolution of electronic orders in the 4d TMOs close to localized-to-itinerant electron crossover.

Based on the above high-pressure resistivity measurements, we constructed in Fig. 4 the T–P phase diagram of $Tl_2Ru_2O_7$ superimposed by the color contour plot of

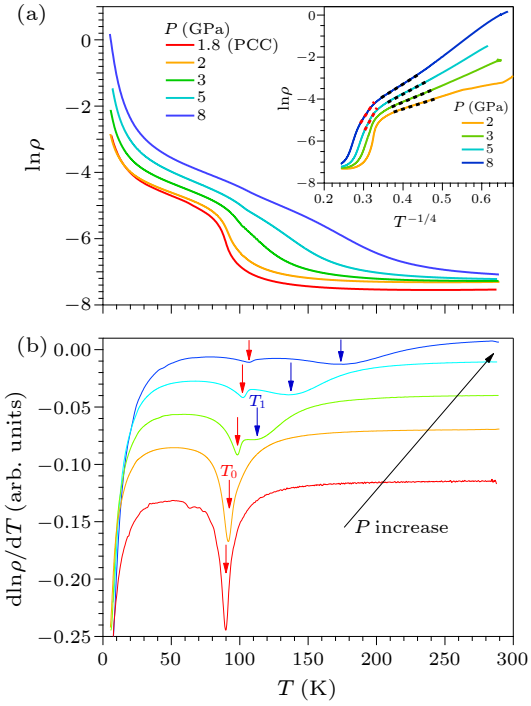

Fig. 3. Temperature dependence of (a) $\ln\rho$ and (b) $\mathrm{d}\ln\rho/\mathrm{d}T$ of $Tl_2Ru_2O_7$ under various hydrostatic pressures up to 8 GPa in CAC. The inset shows the $\ln\rho$ *vs.* $T^{-1/4}$ for the resistivity data. Broken lines represent the linear fitting curves below T_0.

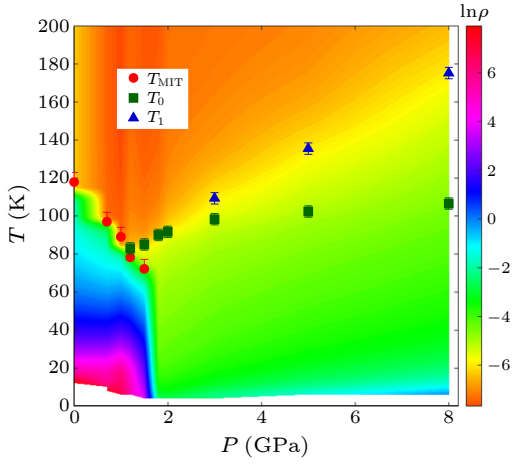

Fig. 4. Temperature-pressure phase diagram of $Tl_2Ru_2O_7$ superimposed by the color contour plot of the $\ln\rho$.

resistivity data in the logarithmic scale. The phase diagram reveals an unusual evolution of the electronic properties of the pyrochlore $Tl_2Ru_2O_7$ featured by a complete suppression of insulating ground state at ∼2 GPa and the concomitant re-emergence of new semiconducting states with two distinct thermally activated regions below T_0 and above T_1 in the pressures range above 2–3 GPa. In the intermediate pressure range 1.2–1.5 GPa, the transition at T_0 takes place slightly higher than T_{MIT}, producing a tricritical-point-like behavior in the phase diagram. The presence of two consecutive phase transitions at T_0 and T_{MIT} in the critical region is consistent with such a scenario with an inhomogeneous electronic state nearby the tricritical point.

To further examine whether the unusual evolutions of transport properties under high pressures are correlated with structural transitions, we performed SXRD measurements of $Tl_2Ru_2O_7$ under pressures up to 15 GPa at room temperature. As seen in Fig. 5(a), all the diffraction peaks can be indexed with the cubic $Fm\bar{3}m$ space group, and they are gradually shifted to higher angles due to the volume shrinkage upon compression. As can be seen, no peaks disappear and new peaks emerge, thus ruling out the structural phase transition below 15 GPa. Here, by fitting the SXRD patterns with the LeBail method, we obtained the lattice constant a and volume V as a function of pressure [see Fig. 5(b)]. The evolution of $V(P)$ can be well fitted by the Birch-Murnaghan equation,

$$P(V) = \frac{3B_0}{2}\left[\left(\frac{V_0}{V}\right)^{7/3} - \left(\frac{V_0}{V}\right)^{5/3}\right] \cdot \left\{1 + \frac{3}{4}(B_0{}' - 4)\left[\left(\frac{V_0}{V}\right)^{2/3} - 1\right]\right\},$$

where V_0 is the unit-cell volume at 0 GPa, B_0 and $B_0{}'$ are the bulk modulus and its derivative with respect to pressure. The calculated B_0 is 166(2) GPa and V_0 is 1054.35(1) Å^3 with fixed $B_0{}' = 4$. The relatively small changes of $\Delta V/V_0$ (∼7% up to 15 GPa) and large bulk modulus indicate that $Tl_2Ru_2O_7$ cannot be easily compressed. Thus, the unconventional evolution of transport properties below 8 GPa should originate from the modifications of electronic states that are sensitive to compression.

Our present study demonstrates that the electronic states of $Tl_2Ru_2O_7$ near the localized-to-itinerant crossover are sensitive to external pressures and exhibit complex evolutions upon compression. Although the application of high pressure can reduce the MIT to some extent, a metallic ground state was not realized as observed in $Hg_2Ru_2O_7$.[29] Instead, the MIT vanishes suddenly at about 1.8 GPa. In addition, it seems that a new electronic order emerges at T_0 prior to the MIT at 1.2–1.5 GPa, resulting in a semiconducting ground state below T_0, which further evolves into two transitions above 3 GPa. In the absence of structural transition, the observations of prominent anomalies in $\rho(T)$ at T_0 and T_1 under high pressures should be attributed to electronic transitions associated with the multiple degrees of freedom. Further studies are needed to determine the exact nature

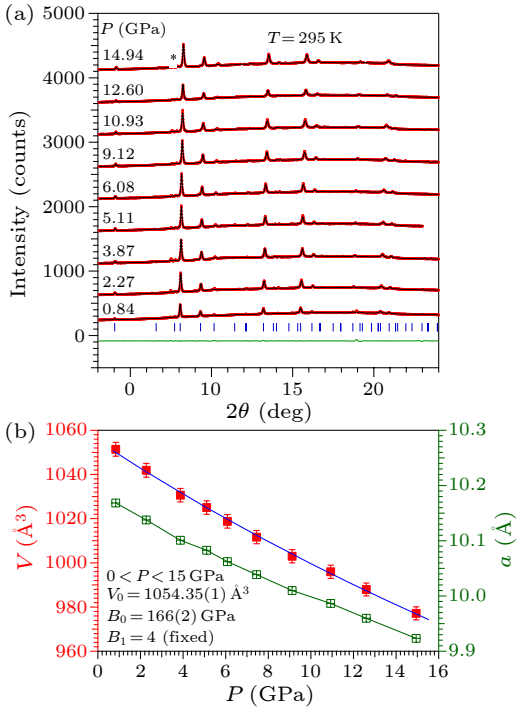

Fig. 5. (a) High-pressure SXRD patterns of $Tl_2Ru_2O_7$ under various pressures up to ∼ 15 GPa. The observed (red circles), calculated (black line), and difference (green line) profiles are shown together with the allowed Bragg reflections (bottom ticks). (b) Pressure dependence of the volume $V(P)$ and lattice constant a. The blue line represents the Birch-Murnaghan fitting to the $V(P)$.

of these electronic orders under high pressure, which may originate from density wave order, structural distortions, or orbital fluctuations. Here we focus on the electrical transport properties and discuss the present results via comparison with other pyrochlore ruthenates and 4d/5d TMOs.

First, the resistivity of $Tl_2Ru_2O_7$ at ambient pressure resembles that of $Hg_2Ru_2O_7$ and $Cd_2Os_2O_7$ featured by a sharp MIT. For $Hg_2Ru_2O_7$, the strong covalency of Hg^{2+} reduced the hybridization between Ru 4d and O 2p orbitals that further narrows the bandwidth of Ru-O derived bands and finally lead to the prominent localization of Ru 4d electrons. Thus, the sharp MIT takes place in concomitant with long-range antiferromagnetic order. For $Cd_2Os_2O_7$, the 5d orbitals with larger spatial expansion can reduce the Coulomb repulsion and enhance the spin–orbital coupling, which further leads to the band renormalization and narrow bandwidth. With the application of pressure to $Hg_2Ru_2O_7$, its MIT is completely suppressed at above 6.5 GPa, resulting in metallic behavior down to the lowest temperature. In contrast to the complete destabilization of the insulating ground state in $Hg_2Ru_2O_7$, the metallic state is avoided in the pressurized $Tl_2Ru_2O_7$ due to the emergence of successive new electronic orders. The emergence of T_0 might originate from the modification of Ru 4d-O 2p derived bands and the hybridization between Ru 4d-Tl 6s orbitals upon compression.

Second, the resistivity curves and VRH plots of $Tl_2Ru_2O_7$ above 2 GPa are similar to that of $Cd_2Ru_2O_7$

under higher pressures over 8 GPa[29] featured by two distinct thermally activated regions, even though the oxidized state of Ru in $Cd_2Ru_2O_7$ (Ru^{5+}) is different from $Tl_2Ru_2O_7$ (Ru^{4+}). Based on the discussion of $Cd_2Ru_2O_7$, the compression of lattice constant might enhance the hybridization of Cd-O that would in turn strengthen the localization of Ru 4d electrons. Then, the opposite effects of the broadening of Ru 4d-O 2p derived energy bands versus the localization of Ru 4d electrons under lattice compression can rationalize the unusual nonmonotonic evolutions of transport properties at high pressures. In such a scenario, the strong electron correlations and Tl 6s states should play an important role in the emergence of novel insulating states of $Tl_2Ru_2O_7$. Further theoretical calculations and experimental investigations are needed to obtain a more comprehensive understanding of the above peculiar electronic behaviors with the electronic dichotomy of localization and itinerancy.

Finally, it is noteworthy that an electronic tricritical point-like behavior can be clearly seen in the phase diagram of $Tl_2Ru_2O_7$, which is similar to the hole-doped FeAs-based superconductors.[8–10,30–34] For example, the FeAs-based system would experience a first order transition from paramagnetic tetragonal phase to collinear antiferromagnetic orthorhombic phase which couples to a nematic order with two-fold rotational symmetry and exhibits superconducting transition. The critical regime strongly involves the coupling among charge, spin, orbital, and lattice degrees of freedom. For $Tl_2Ru_2O_7$ at ambient pressure, the MIT is also accompanied by a concurrent first-order cubic-orthorhombic structural transition, and the modification of Ru-O bond lengths are correlated with the orbital ordering of Ru 4d electrons. In addition, the one-dimensional spin-one Haldane chains with spin gap were proposed to be formed below $T_{\rm MIT}$. Under high pressure, a new insulating state emerges between $T_{\rm MIT}$ and T_0, and further leads to the coexistence of metallic state and two distinct insulating states. The above observations share highly similarity with electronic tricritical point, which exhibits a first-order-like transition with the inhomogeneous electronic phases. Although the nature of these emergent electronic orders at high pressures remains unclear, we hope that the present work can stimulate more studies on this system.

4. Conclusion. In summary, we have successfully synthesized the cubic pyrochlore $Tl_2Ru_2O_7$ under high-pressure and high-temperature conditions and characterized its physical properties at ambient pressure. A sharp metal–insulator transition observed in resistivity is also reflected in magnetic susceptibility and thermopower at ambient pressure. Under high pressures, the metal–insulator transition was gradually reduced and vanished suddenly below 1.8 GPa and two new electronic orders at T_0 and T_1 with unclear origin are observed at pressure above 1.2 GPa and 3 GPa, respectively. Such unusual evolutions of electronic orders under pressures lead to a tricritical-point like behavior in the T–P phase of $Tl_2Ru_2O_7$. Our results demonstrated complex and rich electronic phenomena in the systems close to the localized-to-itinerant electron crossover.

Acknowledgements. This work was supported by the National Key Research and Development Program of China (Grant Nos. 2023YFA1406100 and 2021YFA1400200), the National Natural Science Foundation of China (Grant Nos. 12025408 and 12174424), the Youth Innovation Promotion Association of Chinese Academy of Scineces (Grant No. 2023007). YYJ acknowledges support from the National Natural Science Foundation of China (Grant No. 11904272) and the Open Fund of Hubei Provincial Key Laboratory of Metallurgical Industry Process Systems Science (Grant No. Z202202). The high-pressure resistivity experiments were performed at the Cubic Anvil Cell Station of Synergic Extreme Condition User Facility (SECUF, https://cstr.cn/31123.02.SECUF). High-pressure SXRD measurements were performed at the BL15U1 station of Shanghai Synchrotron Radiation Facility.

References

[1] Sleight A W 1968 *Inorg. Chem.* **7** 9
[2] Shimakawa Y, Kubo Y, Manako T, and Sushko Y 1996 *Nature* **379** 53
[3] Cox P A, Egdell R G, Goodenough J B, Hamnett A, and Naish C C 1983 *J. Phys. C* **16** 6221
[4] Lee S, Park J G, Adroja D T, Khomskii D, Streltsov S, Mcewen K A, Sakai H, Yoshimura K, Anisimov V I, and Mori D 2006 *Nat. Mater.* **5** 471
[5] Hanawa M, Muraoka Y, Tayama T, Sakakibara T, Yamaura J, and Hiroi Z 2001 *Phys. Rev. Lett.* **87** 187001
[6] Reihl B, Riesterer T, Bednorz J G, and Muller K A 1987 *Phys. Rev. B* **35** 8804
[7] Subramanian M A, Ramirez A P, and Kwei G H 1998 *Solid State Ionics* **108** 185
[8] Li Y, Sun Z, Cai J W, Sun J P, Wang B S, Zhao Z Y, Uwatoko Y, Yan J Q, and Cheng J G 2017 *Chin. Phys. Lett.* **34** 087201
[9] Shan P F, Han X, Li X, Liu Z Y, Yang P T, Wang B S, Wang J F, Liu H Y, Shi Y G, and Sun J P 2023 *Mat. Today Phys.* **38** 101267
[10] Sun J P, Jiao Y Y, Yi C J, Dissanayake S E, and Cheng J G 2019 *Phys. Rev. Lett.* **123** 047201
[11] Hou J, Ma H M, Yin Q W, Deng X T, Shan P F, Yang Z R, Uwatoko Y, Yu X H, Ma X L, Shi Y G, Dong X L, Lei H C, Sun J P, and Cheng J G 2025 *Chin. Phys. Lett.* **42** 057403
[12] Ueda K, Fujioka J, Takahashi Y, Suzuki T, Ishiwata S, Taguchi Y, and Tokura Y 2012 *Phys. Rev. Lett.* **109** 136402
[13] Wang R and Sleight A W 1998 *Mater. Res. Bull.* **33** 1005
[14] Kim B J, Jin H, Moon S J, Kim J Y, Park B G, Leem C S, Yu J, Noh T W, Kim C, and Oh S J 2010 *Phys. Rev. Lett.* **101** 076402
[15] Munenaka T and Sato H 2006 *J. Phys. Soc. Jpn.* **75** 10
[16] Manju U, Awana V P S, Kishan H, and Sarma D D 2006 *Phys. Rev. B* **74** 245106
[17] Sleight A W 1974 *Mater. Res. Bull.* **9** 1177
[18] Sleight A W, Gillson J L, Weiher J F, and Bindloss W 1974 *Solid State Commun.* **14** 357
[19] Ito M, Yasui Y, Kanada M, Harashina H, Yoshii S, Murata K, Sato M, Okumura H, and Kakurai K 2001 *J. Phys. Chem. Solids* **62** 337
[20] Park J, Kim K H, Noh H J, Oh S J, Park J H, Lin H J, and Chen C T 2004 *Phys. Rev. B* **69** 165120

[21] Baidya S, Sarkar S, Saha Dasgupta T, and Sarma D D 2012 *Phys. Rev. B* **86** 125117
[22] Tachibana M, Kohama Y, Shimoyama T, Harada A, Taniyama T, Itoh M, Kawaji H, and Atake T 2006 *Phys. Rev. B* **73** 193107
[23] Tachibana M, Kawaji H, and Atake T 2005 *Phys. Rev. B* **71** 060402
[24] Sakai H, Kato M, Yoshimura K, and Kosuge K 2002 *J. Phys. Soc. Jpn.* **71** 422
[25] Mori D, Sonoyama N, Yamada A, Kanno R, Azuma M, Takano M, Suda K, and Ishizawa N 2006 *J. Solid State Chem.* **179** 935
[26] Takeshita N, Terakura C, Tokura Y, Yamamoto A, and Takagi H 2007 *J. Phys. Soc. Jpn.* **76** 063707
[27] Yamamoto A, Sharma P A, Okamoto Y, Nakao A, Katori H A, Niitaka S, Hashizume D, and Takagi H 2007 *J. Phys. Soc. Jpn.* **76** 043703
[28] Lee J S, Lee Y S, Kim K W, Noh T W, Yu J, Takeda Y, and Kanno R 2001 *Physica C* **364** 632
[29] Jiao Y Y, Sun J P, Shahi P, Cui Q, Yu X H, Uwatoko Y, Wang B S, Alonso J A, Weng H M, and Cheng J G 2018 *Phys. Rev. B* **98** 075118
[30] Avci S, Chmaissem W O, Allred J M, Rosenkranz S, Eremin I, Chubukov A V, Bugaris D E, Chung D Y, Kanatzidis M G, Castellan J P, Schlueter J A, Claus H, Khalyavin D D, Manue P, Daoud Aladine A, and Osborn R 2014 *Nat. Commun.* **5** 3845
[31] Waßer F, Schneidewind A, Sidis Y, Wurmehl S, Aswartham S, Büchner B, and Braden M 2015 *Phys. Rev. B* **91** 060505
[32] Böhmer A E, Hardy F, Wang L, Wolf T, Schweiss P, and Meingast C 2015 *Nat. Commun.* **6** 7911
[33] Allred J M, Taddei K M, Bugaris D E, Krogstad M J, Lapidus S H, Chung D Y, Claus H, Kanatzidis M, Brown D E, and Kang J 2016 *Nat. Phys.* **12** 493
[34] Taddei K M, Allred J M, Bugaris D E, Lapidus S H, and Chmaissem O 2016 *Phys. Rev. B* **93** 134510